JOURNAL OF SPACECRAFT AND ROCKETS
Vol. 32, No. 4, July–August 1995

Minimization of Thermoelastic Deformation in Space Structures Undergoing Periodic Motion

Dan Givoli* and Omri Rand†
Technion—Israel Institute of Technology, Haifa 32000, Israel

A numerical scheme is devised for the open-loop optimal control of the thermoelastic deformation of space structures. The motion that the space structure undergoes and the control loads are assumed to be periodic in time, with a given period. Four different cost functionals are considered, which involve the elastic deformation of the structure and include penalties on the control magnitudes. A finite element harmonic balance procedure is employed as the first step of the optimization scheme. The performance of the scheme is demonstrated via numerical examples.

Nomenclature

A	= cross-sectional area
C	= cost functional
c	= specific heat
E	= Young's modulus
F	= integrand in cost functional
$\boldsymbol{F}$	= load vector
$\boldsymbol{G}$	= capacity matrix
K	= number of observation points
$\boldsymbol{K}$	= stiffness matrix
k	= thermal conductivity
M	= number of control forces
$\boldsymbol{M}$	= mass matrix
P_m	= control forces
${}^nP_m$	= nth Fourier coefficient of control force P_m
$\boldsymbol{P}$	= conductivity matrix
p	= perimeter of the member's cross section
$\boldsymbol{Q}$	= thermal load vector
q	= given time-periodic incident flux
$\boldsymbol{R}$	= radiation vector
r_m	= force weights in cost functional
s	= axial coordinate along the rod
$T(\boldsymbol{x}, \phi)$	= temperature
T_{ref}	= reference temperature in which the truss is undeformed
$\boldsymbol{T}$	= temperature vector
t	= time
$\boldsymbol{u}$	= displacement vector
$\boldsymbol{u}^T$	= displacement vector due to thermal effects
$\boldsymbol{u}^{1_m}$	= displacement vector due to the action of load P_m with unit Fourier coefficients
u_i	= displacement components
w, w_k	= displacement weights in cost functional
$\boldsymbol{x}$	= location of point in the structure
α	= coefficient of thermal expansion
ϵ	= surface emissivity of the truss member
ρ	= mass density
σ	= universal Stefan–Boltzmann constant
ϕ	= azimuth angle
Ω	= structure domain

I. Introduction

THE design process of space structures usually involves large-scale thermal and thermoelastic numerical analyses. Solar radiation and radiation from other sources induce a temperature field in the structure, which in turn generates an elastic displacement field. The latter is often very important to the designer, for two main reasons. First, the displacements must usually satisfy certain limitations dictated by the allowed working conditions of various instruments and antennas. For example, a parabolic reflector may cease to be effective when undergoing large deflection.[1] Second, the strain energy absorbed may affect the rigid-body dynamical behavior of the structure. In fact, elastic vibrations due to momentary activation of engines may cause undesired changes in the paths of satellites leading to the loss of their stability.[2]

The mathematical problems modeling the thermal behavior of space structures are usually highly nonlinear due to the presence of thermal radiation emitted by the structure and to nonlinear material behavior. A further complication is introduced when part of the structure overshadows another part of it. For an overview of the factors involved in this type of analysis see Refs. 3–7. Various numerical methods have been devised for the thermoelastic analysis of space structures. These include methods for the one-dimensional analysis of space trusses[8,9] and for the two-dimensional (cross-sectional) and three-dimensional analyses of frame structures.[10–13]

In Refs. 14 and 15 we have considered space structures undergoing periodic motion. Periodic motion is typical of structures that spin around a certain axis for stabilization purposes and structures such as satellites that orbit around the Earth. Such motion gives rise to a time-periodic temperature field, which in turn induces time-periodic elastic deformation in the structure. To find these two fields, a numerical method is devised in Refs. 14 and 15, based on the combination of finite element analysis in space and spectral (Fourier) analysis in time. This method is shown to be very effective in a variety of configurations.

This paper concerns the open-loop optimal control of the thermoelastic deformation of a space structure undergoing a periodic motion. The optimal control of space structures in general is an active field of research; e.g., see Refs. 16–18, the collections of papers in Refs. 19 and 20, and references therein. The thermoelastic deformation may be controlled by selecting materials with appropriate properties (passive control), or by controlling the temperature distribution in the structure, or by using control loads that are applied by actuators and that directly control the elastic deformation.

There has been a much smaller body of research, however, on optimal control under time-periodic conditions. It includes the works by Speyer,[21] Speyer and Evans,[22] Wang and Speyer,[23] and Gilbert.[24] In Ref. 21, the analysis of aircraft trajectories was performed, and periodic controls were shown to improve the fuel performance over static cruise in certain cases. In Refs. 22–24, the necessary and sufficient conditions for a periodic process to be a local minimum are considered in a general setting, as well as the ways to produce this optimal process.

Here we use the thermoelastic analysis method devised in Refs. 14 and 15 as the first step of an open-loop optimal control scheme. Both the motion of the structure and the control loads are assumed to be periodic in time, with a given period. The open-loop control

Received Nov. 18, 1992; revision received May 15, 1993; accepted for publication June 1, 1993.

*Senior Lecturer, Department of Aerospace Engineering.
†Associate Professor, Department of Aerospace Engineering.

is aimed at minimizing the average thermoelastic deformation during one period. The minimization criterion is based on one of four different cost functionals, which involve the elastic deformation of the structure and include penalties on the control magnitudes. The proposed optimization scheme is extremely compatible with the harmonic finite element method of analysis used in Refs. 14 and 15. We consider some theoretical issues associated with the new scheme and give some numerical examples to demonstrate its performance.

II. Optimal Control Scheme

Consider a flexible space structure undergoing periodic motion. The periodicity may originate, for example, from the fact that the structure orbits around the Earth or that the structure spins around a certain axis. The period is given to be $2\pi/\omega$, where ω is the circular frequency of the motion. The domain occupied by the structure is denoted Ω. The structure is exposed to incident solar radiation, which induces a time-dependent temperature field $T(\boldsymbol{x}, t)$ in it. Here $\boldsymbol{x}$ is the position vector with respect to a Cartesian coordinate system (x, y, z) fixed to (and rotating with) the structure. Since the motion is periodic, it is convenient to define the azimuth angle $\phi = \omega t$ and to use the nondimensional variable $\phi \in [0, 2\pi]$ instead of the time t. Thus, we write the temperature field as $T(\boldsymbol{x}, \phi)$.

This temperature field, in turn, induces a time-dependent elastic displacement vector field. The dynamic elastic deformation of space structures is usually undesirable, for the reasons explained previously. To reduce the temperature-induced deformation, we applied a number of time-periodic external concentrated forces, with chosen orientations, as controllers at some given points on the surface of the structure. There are M such control forces, denoted $P_1(\phi), P_2(\phi), \ldots, P_M(\phi)$. These forces remain fixed to the structure in location and orientation as the structure rotates. See the setup illustrated in Fig. 1.

We shall assume here that the structure represented by Ω is attached to a much larger and more rigid space structure, so that the control forces, applied by actuators, can be regarded as external to the system under investigation. Although this is a fairly restrictive assumption, there are important cases where it may be regarded as reasonable, as for example, in the case of a flexible antenna mounted on a large space platform. Of course, the assumption that the large structure may be replaced by the condition of rigid supports on the interface is justified only if the difference between the rigidities of the two structures is sufficiently large. We also assume that each control force acting on the smaller structure has an equal and opposite force applied to the larger structure, so that the entire system is self-equilibrated and no rigid-body motion results. A possible way to extend the present approach would be to consider the entire free-floating space structure, while restricting the applied forces to always be self-equilibrated. (We thank the reviewer for suggesting this extension to us.)

We remark that in reality the number of control forces M should typically be small, since the additional structure and mechanisms necessary to apply these forces to control the thermal deformation effectively may become heavy and complex. In addition, some limits must be imposed on the amplitude of these forces and sometimes also on the rate in which they can be changed in time. One must take these feasibility constraints into account when considering an optimal control solution.

We denote $\boldsymbol{u}(\boldsymbol{x}, \phi)$ the displacement vector field generated by both the temperature field and by the collective action of all of the control loads. We denote the three components of $\boldsymbol{u}$, in three chosen orthogonal directions, by $u_j(\boldsymbol{x}, \phi)$. For example, the u_j may stand for u_x, u_y, and u_z or alternatively for u_r, u_θ, and u_z (in the directions corresponding to a given cylindrical coordinate system).

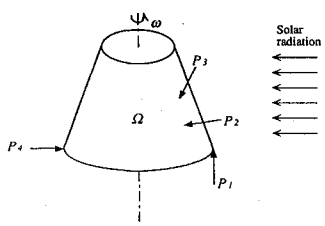

Fig. 1 Space structure in periodic motion, loaded by thermal loads and by a number of time-periodic concentrated control forces.

The problem is now to determine the optimal control forces $P_m(\phi), m = 1, \ldots, M$, so as to minimize the deformation. More precisely, we consider the minimization of a cost functional of the form

$$C = \frac{1}{2\pi} \int_0^{2\pi} F(\boldsymbol{u}; \phi)\, \mathrm{d}\phi \tag{1}$$

where the integrand F may be one of the following:

Cost A:

$$F = \sum_{k=1}^{K} w_k [u_j(\boldsymbol{x}_k, \phi)]^2 + \sum_{m=1}^{M} r_m [P_m(\phi)]^2 \tag{2}$$

Cost B:

$$F = \sum_{k=1}^{K} w_k |\boldsymbol{u}(\boldsymbol{x}_k, \phi)|^2 + \sum_{m=1}^{M} r_m [P_m(\phi)]^2 \tag{3}$$

Cost C:

$$F = \int_\Omega w(\boldsymbol{x}) [u_j(\boldsymbol{x}, \phi)]^2\, \mathrm{d}\Omega + \sum_{m=1}^{M} r_m [P_m(\phi)]^2 \tag{4}$$

Cost D:

$$F = \int_\Omega w(\boldsymbol{x}) |\boldsymbol{u}(\boldsymbol{x}, \phi)|^2\, \mathrm{d}\Omega + \sum_{m=1}^{M} r_m [P_m(\phi)]^2 \tag{5}$$

In Eqs. (2–5), the w_k and r_m are given real non-negative constants, and $w(\boldsymbol{x})$ is a given real non-negative function.

The interpretation of these four cost functionals is as follows. In all four cases, the cost is the time average over one time period, as implied by Eq. (1), of a certain combination of deformation and loads. Costs A and B involve the displacements at K given observation points $\boldsymbol{x}_k$, for $k = 1, \ldots, K$. The quantity to be minimized includes the weighted sum of the squares of the displacements at all of the observation points [the first sums in Eqs. (2) and (3)]. A penalty on the magnitudes of the control forces is added, by summing the weighted force squares [the second sums in Eqs. (2) and (3)]. The difference between costs A and B is that in cost A the displacement component u_j, in a certain chosen direction j, is minimized, whereas in cost B it is the "total" displacement $|\boldsymbol{u}|$ that is minimized. Costs C and D are analogous to costs A and B, respectively; only the sums in Eqs. (2) and (3) over a finite number of discrete observation points are replaced by an integral over the entire structure domain Ω. The integrand is the weighted square of either a given displacement component (cost C) or the total displacement (cost D).

Now we present a numerical scheme for the minimization of these cost functionals. The scheme is based on the assumption that the elastic response of the structure can be regarded as linear. Thus, it is assumed that the structure material is linearly elastic and that the deformation is small. These assumptions should be justified a posteriori by checking the displacements resulting from the calculations. In addition, we assume for simplicity that no energy dissipation (damping) mechanism exists in the structure. We note, however, that, although the linearity assumption is crucial, the scheme can be easily generalized to include damping effects.

We denote the displacement vector field due to thermal effects alone,i.e., before the activation of any control load, by $\boldsymbol{u}^T(\boldsymbol{x}, \phi)$. We also denote the displacement field due to the action of the single force P_m, by $\boldsymbol{u}^{P_m}(\boldsymbol{x}, \phi)$. Using superposition, it is clear that

$$\boldsymbol{u}(\boldsymbol{x}, \phi) = \boldsymbol{u}^T(\boldsymbol{x}, \phi) + \sum_{m=1}^{M} \boldsymbol{u}^{P_m}(\boldsymbol{x}, \phi) \tag{6}$$

Next, we represent all of the functions in Eq. (6) by their complex Fourier series expansions. To this end, given a periodic function $y(\phi)$, we denote by ${}^n y$ its nth Fourier coefficient:

$$y(\phi) = \sum_{n=-\infty}^{\infty} {}^n y e^{in\phi} \tag{7}$$

$${}^n y = \frac{1}{2\pi} \int_0^{2\pi} e^{-in\phi} y(\phi)\, d\phi \tag{8}$$

Here $i = \sqrt{-1}$. Thus we write Eq. (6) as

$$\boldsymbol{u}(x, \phi) = \sum_{n=-\infty}^{\infty} {}^n\boldsymbol{u}^T(x) e^{in\phi} + \sum_{m=1}^{M} \sum_{n=-\infty}^{\infty} {}^n\boldsymbol{u}^{P_m}(x) e^{in\phi} \tag{9}$$

We also expand the load function $P_m(\phi)$ in a Fourier series:

$$P_m(\phi) = \sum_{n=-\infty}^{\infty} {}^n P_m e^{in\phi} \tag{10}$$

In addition, we define the vector field $\boldsymbol{u}^{1m}(x, \phi)$ as the displacement due to the single load P_m, where all of the Fourier coefficients of P_m are chosen to be unity. In other words, $\boldsymbol{u}^{1m}$ is the displacement generated by the special force $P_m(\phi) = \sum_{n=-\infty}^{\infty} e^{in\phi}$. We expand $\boldsymbol{u}^{1m}$ in a Fourier series, i.e.,

$$\boldsymbol{u}^{1m} = \sum_{n=-\infty}^{\infty} {}^n\boldsymbol{u}^{1m} e^{in\phi} \tag{11}$$

Now, it is easy to show that, for each n separately,

$${}^n\boldsymbol{u}^{P_m} = {}^n P_m\, {}^n\boldsymbol{u}^{1m} \tag{12}$$

This relation follows from the linearity of the problem as well as from the no-damping assumption. Linearity implies that any two different Fourier modes, $e^{in\phi}$ and $e^{il\phi}$ with $|n| \neq |l|$, do not interact. The no-damping assumption implies that the two modes $e^{in\phi}$ and $e^{-in\phi}$ do not interact either. (In the terminology of real Fourier series this means that without damping there is no coupling between the sine and cosine terms. Thus, a sine loading will generate only a sine displacement.) As noted previously, the scheme can easily be extended to include damping effects, although the linearity assumption cannot be relaxed.

We substitute Eq. (12) in Eq. (9) to obtain, after rearranging,

$$\boldsymbol{u}(x, \phi) = \sum_{n=-\infty}^{\infty} e^{in\phi} \left[{}^n\boldsymbol{u}^T(x) + \sum_{m=1}^{M} {}^n P_m\, {}^n\boldsymbol{u}^{1m}(x) \right] \tag{13}$$

Written for each component separately, Eq. (13) becomes

$$u_j(x, \phi) = \sum_{n=-\infty}^{\infty} e^{in\phi} \left[{}^n u_j^T(x) + \sum_{m=1}^{M} {}^n P_m\, {}^n u_j^{1m}(x) \right] \tag{14}$$

The only unknown variables on the right-hand sides of Eqs. (13) and (14) are the load Fourier coefficients ${}^n P_m$, for $m = 1, \ldots, M$ and $n = 0, \pm 1, \pm 2, \ldots$. The functions $\boldsymbol{u}^T$ and $\boldsymbol{u}^{1m}$ are assumed to be known, having been found by using some numerical analysis method (see the next section). Their Fourier coefficients, ${}^n\boldsymbol{u}^T$ and ${}^n\boldsymbol{u}^{1m}$, are determined either directly (as in the numerical method used in the next section) or by applying the fast Fourier transform (FFT) to $\boldsymbol{u}^T$ and $\boldsymbol{u}^{1m}$.

We now substitute Eqs. (14) [or (13)] and (10) into one of the four cost functionals given earlier. Having made this substitution, the cost functional C becomes a quadratic function of the parameters ${}^n P_m$. To minimize the cost we make use of the necessary condition for a stationary point, namely, the condition that the derivative of the cost with respect to each of the ${}^n P_m$ must vanish. This yields a linear system of algebraic equations for the constants ${}^n P_m$, for each n separately. An additional calculation that involves the second derivatives of C shows that the sufficient condition for a minimum is satisfied, and thus the corresponding value of C is indeed a minimum.

We outline the calculation involved in this process for cost A. Substituting Eqs. (14) and (10) into Eq. (2) yields

$$F = \sum_{k=1}^{K} w_k \left[\sum_{n=-\infty}^{\infty} e^{in\phi} \left({}^n u_j^T + \sum_{m=1}^{M} {}^n P_m\, {}^n u_j^{1m} \right) \right]^2 + \sum_{m=1}^{M} r_m \left[\sum_{n=-\infty}^{\infty} {}^n P_m e^{in\phi} \right]^2 \tag{15}$$

Now we differentiate Eq. (15) with respect to ${}^n P_m$ and apply the operator $(1/2\pi) \int_0^{2\pi} d\phi$ as in Eq. (1), to get

$$\frac{\partial C}{\partial ({}^n P_m)} = \sum_{k=1}^{K} w_k\, {}^n u_j^{1m} \left({}^n u_j^T + \sum_{l=1}^{M} {}^n P_l\, {}^n u_j^{1l} \right) + r_m\, {}^n P_m \tag{16}$$

In obtaining Eq. (16), we made use of the orthogonality property of the $e^{in\phi}$ functions. Now, requiring $\partial C / \partial ({}^n P_m) = 0$, Eq. (16) yields a linear system of equations for the constants ${}^n P_m$. In matrix notation, we get the following:

Cost A:

$${}^n\boldsymbol{A}\, {}^n\boldsymbol{P} = {}^n\boldsymbol{b} \tag{17}$$

where

$${}^n\boldsymbol{A} = [{}^n A_{ml}]; \qquad {}^n\boldsymbol{P} = \{{}^n P_m\}; \qquad {}^n\boldsymbol{b} = \{{}^n b_m\} \tag{18}$$

$${}^n A_{ml} = r_l \delta_{ml} + \sum_{k=1}^{K} w_k\, {}^n u_j^{1m}(x_k)\, {}^n u_j^{1l}(x_k) \tag{19}$$

$${}^n b_m = -\sum_{k=1}^{K} w_k\, {}^n u_j^{1m}(x_k)\, {}^n u_j^T(x_k) \tag{20}$$

In Eq. (19), δ_{ml} is the Kronecker delta. The M-by-M system given by Eq. (17) must be solved for each n separately.

Similarly, we get analogous results for costs B, C, and D. Equations (17) and (18) remain unchanged, whereas the entries of the matrix ${}^n\boldsymbol{A}$ and the vector ${}^n\boldsymbol{b}$ are as follows:

Cost B:

$${}^n A_{ml} = r_l \delta_{ml} + \sum_{k=1}^{K} w_k\, {}^n\boldsymbol{u}^{1m}(x_k) \cdot {}^n\boldsymbol{u}^{1l}(x_k) \tag{21}$$

$${}^n b_m = -\sum_{k=1}^{K} w_k\, {}^n\boldsymbol{u}^{1m}(x_k) \cdot {}^n\boldsymbol{u}^T(x_k) \tag{22}$$

Cost C:

$${}^n A_{ml} = r_l \delta_{ml} + \int_\Omega w(x)\, {}^n u_j^{1m}(x)\, {}^n u_j^{1l}(x)\, d\Omega \tag{23}$$

$${}^n b_m = -\int_\Omega w(x)\, {}^n u_j^{1m}(x)\, {}^n u_j^T(x)\, d\Omega \tag{24}$$

Cost D:

$${}^n A_{ml} = r_l \delta_{ml} + \int_\Omega w(x)\, {}^n\boldsymbol{u}^{1m}(x) \cdot {}^n\boldsymbol{u}^{1l}(x)\, d\Omega \tag{25}$$

$${}^n b_m = -\int_\Omega w(x)\, {}^n\boldsymbol{u}^{1m}(x) \cdot {}^n\boldsymbol{u}^T(x)\, d\Omega \tag{26}$$

In Eqs. (21), (22), (25), and (26), we have used $\boldsymbol{x} \cdot \boldsymbol{y}$ to denote the scalar (dot) product between the vectors $\boldsymbol{x}$ and $\boldsymbol{y}$.

Now we make a number of remarks regarding the scheme proposed earlier.

Remark 1: The cost integrands given by Eqs. (2–5) involve the elastic displacements. Cost functionals that involve the stresses in the structure can be considered as well. If a certain stress component is to be minimized, a cost analogous to previous cost A or cost C may be used. In that case, the final linear system consists of equations analogous to Eqs. (17–20) or (23) and (24). A typical example is that of a truss-type structure, in which the only significant stress component is the axial one. However, in most large flexible space structures the stresses are small, and the control of the elastic deformation is considered more critical. Yet another possibility is to minimize the strain energy contained in the structure. Also, penalties may be imposed on the power (energy per unit time) of the applied controls, in addition to the penalties on the load magnitudes.

Remark 2: One may wonder whether it would be legitimate to write a Fourier series expansion for $|\boldsymbol{u}|$ analogous to Eq. (9) and then to use it directly in Eqs. (3) and (5) rather than follow the procedure we have used. The answer is negative. The superposition principle, which was used to obtain Eq. (9), applies to $\boldsymbol{u}$ but not to $|\boldsymbol{u}|$, since the latter is not a displacement component in a fixed direction.

Remark 3: It is possible to use different weights w_k, r_m, and $w(\boldsymbol{x})$ for different modes. In this case, these parameters are replaced by ${}^n w_k, {}^n r_m$, and ${}^n w(\boldsymbol{x})$ in Eqs. (19–26). Such a procedure, although ad hoc in nature, may provide better control of certain modes (say, the lower ones) at the expense of other modes that may be considered less important from the design viewpoint.

Remark 4: Consider the special case where cost A is used, with $M = K$, and $r_m = 0$ for all m. The condition $M = K$ means that the number of controls forces is equal to the number of observation points, and $r_m = 0$ means that no penalty is imposed on the magnitude of the controls. In this special case it can be shown that the use of the optimal control yields zero displacement u_j at all of the observation points $\boldsymbol{x}_k$. We show this for the simplest case, namely, $M = K = 1$ (one control and one observation point). In this case Eqs. (17–20) reduce to

$$ {}^nP = -\frac{{}^n u_j^T(\boldsymbol{x}_1)}{{}^n u_j^{1_1}(\boldsymbol{x}_1)} \tag{27} $$

The denominator in Eq. (27) never vanishes if the control force has any effect on the observable displacement. From Eqs. (14) and (27) we have

$$ u_j(\boldsymbol{x}_1, \phi) = \sum_{n=-\infty}^{\infty} e^{in\phi}\left[{}^n u_j^T(\boldsymbol{x}_1) - \frac{{}^n u_j^T(\boldsymbol{x}_1)}{{}^n u_j^{1_1}(\boldsymbol{x}_1)} {}^n u_j^{1_1}(\boldsymbol{x}_1)\right] = 0 \tag{28} $$

namely, the displacement u_j vanishes at the observation point.

To show that this result holds true for the case $M = K > 1$ as well, we consider Eq. (14) again. We set $\boldsymbol{x} = \boldsymbol{x}_k$ in Eq. (14) and require $u_j(\boldsymbol{x}_k, \phi) = 0$. Then for each n Eq. (14) becomes an homogeneous linear system of K equations and M unknowns. If $M = K$, and assuming that the coefficient matrix is nonsingular, the only solution to this system is the trivial one. (A singular coefficient matrix corresponds to the case where the system is not controllable, e.g., when the application of one of the control loads does not affect at all a certain part of the structure.) Thus, a zero-displacement solution is achieved. Moreover, it is clear that this solution is also the minimizer to cost A, provided that all of the r_m are set to zero.

To summarize, in this particular case it is possible to totally annihilate the displacement component u_j at all of the observation points. The price one has to pay to achieve this is in the magnitude of the control loads and/or in the displacements at points other than the observation points. See Sec. IV for a numerical investigation of this issue. We also note that this situation is unique to cost A.

Remark 5: Consider the special case where cost A is used, with $M > K$ and $r_m = 0$ for all m. This case is similar to the one considered earlier, only now there are more control loads than observation points. The consequence of this is that the matrix ${}^n\boldsymbol{A}$, whose entries are given in Eq. (19), becomes singular. This is quite expected in the light of the previous remark; one cannot do better than to make all observable displacements vanish, as in the case $M = K$. Thus, if cost A is used and $r_m = 0$, it is superfluous to apply more control forces than observation points. We demonstrate this in the case $K = 1$ and $M = 2$. From Eq. (19) we get

$$ {}^n\boldsymbol{A} = w_1 \begin{bmatrix} \left({}^n u_j^{1_1}\right)^2 & {}^n u_j^{1_1}\, {}^n u_j^{1_2} \\ {}^n u_j^{1_2}\, {}^n u_j^{1_1} & \left({}^n u_j^{1_2}\right)^2 \end{bmatrix} \tag{29} $$

This matrix is clearly singular, since its determinant is zero. As before, this situation is unique to cost A.

Remark 6: In practice, only a finite usually small, number of models is taken into account in the calculation, relying on the assumption that the Fourier series expansion Eq. (10) of the control force P_m converges rapidly. This assumption precludes rapidly varying controls such as bang-bang type ones. To justify the supposition that Eq. (10) converges at all, we again consider the very simple formula given in Eq. (27). The denominator, ${}^n u_j^{1_1}$, is by definition the displacement amplitude due to unit-amplitude loading. An asymptotic calculation for a simple spring-mass model shows that ${}^n u_j^{1_1} \sim -1/(\rho n^2)$ as $|n| \to \infty$. On the other hand, the numerator of Eq. (27), ${}^n u_j^T$, is the displacement amplitude due to thermal loading whose own amplitude is typically rapidly decreasing as $|n| \to \infty$. Therefore, ${}^n u_j^T \sim -1/(\rho|n|^{2+\beta})$, where $\beta > 0$. From Eq. (27) we thus get $|{}^nP| \sim |n|^{-\beta}$ as $|n| \to \infty$, and hence $\lim_{|n|\to\infty} P_n = 0$. Numerical experiments show that usually the control forces decrease rapidly in magnitude as $|n|$ becomes large.

Remark 7: Finally, we discuss the evaluation of the integrals appearing in Eqs. (23–26) for costs C and D. We assume that the functions ${}^n u_j^{1_m}(\boldsymbol{x})$ and ${}^n u_j^T(\boldsymbol{x})$ were obtained by using the finite element method (see the next section). Thus, these functions can be written as linear combinations of the finite element shape functions[25] $N_A(\boldsymbol{x})$:

$$ {}^n u_j^{1_m}(\boldsymbol{x}) = \sum_{A=1}^{N_{np}} \left({}^n d_j^{1_m}\right)_A N_A(\boldsymbol{x}) \tag{30} $$

$$ {}^n u_j^T(\boldsymbol{x}) = \sum_{A=1}^{N_{np}} \left({}^n d_j^T\right)_A N_A(\boldsymbol{x}) \tag{31} $$

Here the index A stands for a node number, and N_{np} is the total number of nodal points in the finite element mesh. The constants $({}^n d_j^{1_m})_A$ and $({}^n d_j^T)_A$ are the nodal values of ${}^n u_j^{1_m}(\boldsymbol{x})$ and ${}^n u_j^T(\boldsymbol{x})$ and are the entries of the N_{np}-dimensional vectors ${}^n\boldsymbol{d}_j^{1_m}$ and ${}^n\boldsymbol{d}_j^T$, which are computed by the finite element code. We also define the N_{np}-by-N_{np} matrix $\boldsymbol{M}$, whose entries are given by

$$ M_{AB} = \int_\Omega N_A w N_B \, d\Omega \tag{32} $$

In the context of elastodynamics, the matrix $\boldsymbol{M}$ is known as the finite element mass matrix, where the weight function $w(\boldsymbol{x})$ plays the role of the mass density. If w is assumed to be constant in each element, then forming $\boldsymbol{M}$ for various types of shape functions N_A is standard.[25]

Now we substitute Eqs. (30) and (31) into Eqs. (23–26) and obtain the following expressions for the entries of ${}^n\boldsymbol{A}$ and ${}^n\boldsymbol{b}$:

Cost C:

$$ {}^nA_{ml} = r_l\delta_{ml} + {}^n\boldsymbol{d}_j^{1_m} \cdot \boldsymbol{M}\, {}^n\boldsymbol{d}_j^{1_l} \tag{33} $$

$$ {}^nb_m = -{}^n\boldsymbol{d}_j^{1_m} \cdot \boldsymbol{M}\, {}^n\boldsymbol{d}_j^T \tag{34} $$

Cost D:

$$ {}^nA_{ml} = r_l\delta_{ml} + \sum_{j=1}^{3} {}^n\boldsymbol{d}_j^{1_m} \cdot \boldsymbol{M}\, {}^n\boldsymbol{d}_j^{1_l} \tag{35} $$

$$ {}^nb_m = -\sum_{j=1}^{3} {}^n\boldsymbol{d}_j^{1_m} \cdot \boldsymbol{M}\, {}^n\boldsymbol{d}_j^T \tag{36} $$

The matrix-vector products in Eqs. (33–36) should be implemented so as to exploit the sparse structure that the matrix $\boldsymbol{M}$ typically possesses.

III. Thermal and Thermoelastic Analyses

The optimization scheme presented in the previous section makes use of the Fourier coefficients of the two functions $\boldsymbol{u}^T(x, \phi)$ and $\boldsymbol{u}^{1m}(x, \phi)$, which were assumed to be given. Now we consider the numerical method used to obtain these two functions. The former is harder to obtain, since one must first compute the temperature field $T(x, \phi)$. Altogether, one has to perform one thermal analysis (to obtain T), one thermoelastic analysis (to obtain $\boldsymbol{u}^T$), and M purely elastic analyses (to obtain $\boldsymbol{u}^{1m}$ for $m = 1, \ldots, M$).

If some standard numerical method, such as finite element spatial discretization and time integration, is employed to obtain $\boldsymbol{u}^T$ and $\boldsymbol{u}^{1m}$, then their Fourier coefficients can be found by using an FFT scheme. Alternatively, and preferably, one may use the numerical method of analysis proposed in Refs. 14 and 15, which directly provides the Fourier coefficients of the two functions. Following is a brief description of this method.

To fix ideas, we consider a three-dimensional truss structure exposed to an incoming heat flux and undergoing periodic motion with a period of $2\pi/\omega$. The truss members, which are straight rods connected by joints, emit radiation into space. The thermal analysis is based on the following differential equation, which is assumed to hold in each truss member[14]:

$$\omega\rho c\frac{\partial T}{\partial \phi} = \frac{\partial}{\partial s}\left(k\frac{\partial T}{\partial s}\right) - C_R T^4 + q \tag{37}$$

where T is the unknown temperature field, C_R is the radiation coefficient, and C_R and q are given by

$$C_R = \sigma\epsilon(p/A), \qquad q(\phi) = \alpha_s\beta(\phi)(p/A)q_{\text{sun}} \tag{38}$$

where α_s is the surface absorptivity, $\beta(\phi)$ is the so-called view factor associated with the member, and q_{sun} is the magnitude of the solar radiation. For a large opaque structure with a complicated geometry, the determination of the view factor $\beta(\phi)$ in Eq. (38) is not trivial. One may use the general algorithm given in Ref. 15 to this end.

The elastic displacement field u is governed by the linear equation

$$\omega^2\rho A\frac{\partial^2 u}{\partial \phi^2} = \frac{\partial}{\partial s}\left[EA\left(\frac{\partial u}{\partial s} - f_T\right)\right] + f_C \tag{39}$$

where f_T is the thermoelastic loading, and f_C is the centrifugal loading. If thermal effects are considered, then $f_T = \alpha(T - T_{\text{ref}})$. If no temperature effects are considered, f_T is zero. The load f_C is either the axial component of the centrifugal force $\rho A\omega^2 r$ (where r is the distance from the axis of spin), if the periodicity of the motion originates from the spinning of the structure, or zero otherwise.

A consistent finite element spatial discretization is now applied to Eqs. (37) and (39). This procedure, known as semidiscretization,[25] leads to the two following systems of ordinary differential equations in the angle ϕ (or in time)[14]:

Thermal:

$$\boldsymbol{G}\dot{\boldsymbol{T}}(\phi) + \boldsymbol{P}\boldsymbol{T}(\phi) + \boldsymbol{R}[\boldsymbol{T}(\phi)] = \boldsymbol{Q}(\phi) \tag{40}$$

Elastic:

$$\boldsymbol{M}\ddot{\boldsymbol{d}}(\phi) + \boldsymbol{K}\boldsymbol{d}(\phi) = \boldsymbol{F}[\boldsymbol{T}(\phi), \phi] \tag{41}$$

Here a dot indicates differentiation with respect to ϕ. In Eq. (40), the vector $\boldsymbol{T}$ contains the unknown nodal values of the temperature, and $\boldsymbol{R}$ depends nonlinearly on the temperature vector $\boldsymbol{T}$. In Eq. (41), $\boldsymbol{d}$ contains the unknown displacements at the nodes in the directions x, y, and z. In both Eqs. (40) and (41), periodic solutions with period $2\pi/\omega$ are sought.

The semidiscrete systems equations (40) and/or (41) have to be solved next. If the problem at hand is purely elastic, the system equation (41) is solved directly. On the other hand, if thermal effects are present, then the system equation (40) has to be solved first for the temperature vector $\boldsymbol{T}(\phi)$. Then $\boldsymbol{T}(\phi)$ is substituted in the right-hand side of equation (41), which is solved to yield the displacement vector $\boldsymbol{d}(\phi)$.

The method of solution is based on the discrete Fourier decomposition of each ϕ-dependent function in Eqs. (40) and (41) into a finite number of harmonics N. In others words, if $\boldsymbol{f}(t)$ is any vector variable appearing in Eq. (40) or Eq. (41), then it is approximately represented by the finite Fourier expansion,

$$\boldsymbol{f}(\phi) \simeq \sum_{n=-N}^{N} {}^n\boldsymbol{f}e^{in\phi} \tag{42}$$

Expressions such as Eq. (42) are used for all of the variables in Eqs. (40) and (41). The calculations involving arithmetic manipulation of the Fourier series representations [Eq. (42)] are all performed symbolically by the computer code itself, in the manner explained in Ref. 14. Then, from Eqs. (40) and (41) one obtains a system of algebraic equations for the unknown coefficient vectors ${}^n\boldsymbol{T}$ and ${}^n\boldsymbol{d}$, $n = 1, \ldots, N$. Equation (40) yields a nonlinear algebraic system of equations, which is solved via a Newton Raphson type iterative procedure, whereas Eq. (41) yields a linear algebraic system of equations, whose dimension is about three times larger than that of its thermal counterpart, and which is solved by standard Gauss elimination. Consult Refs. 14 and 15 for further details.

IV. Numerical Experiments

The numerical optimal control scheme is now applied to the simple cylindrically shaped truss structure illustrated in Fig. 2. The structure spins around its axis with an angular speed of $\omega = 5\times10^{-5}$ rad/s, which is slightly larger than the typical speed corresponding to a quasisteady motion,[15] while being exposed to incident solar radiation. The two ends of the cylinder are assumed to be fixed to rigid bases, so that they are constrained to rotate without deformation. The structure is made of a composite graphite/epoxy material, whose thermal and mechanical properties are $\rho c = 1.76\times10^6$ J/m^3 K, $k = 10.1$ W/m K, $C_R = 9.1\times10^{-7}$ W/m^3 K^4, $\alpha_s = 0.92$, $\rho A = 51.3$ kg/m, $EA = 1.41\times10^6$ N, $\alpha = 7.3\times10^{-7}$ 1/K. Other parameters are $q_{\text{sun}} = 1300$ W/m^2, $T_{\text{ref}} = 299$ K, and $p/A = 20$ m^{-1}.

The cylinder is of length 6 m and radius 1.4 m. It is assumed to be covered with an opaque material, so self-shadowing effects are present. Each truss member is represented by one finite element with linear shape functions. Altogether there are 170 rods (=elements) and 50 joints (=nodes) in the structure. The Cartesian coordinate system (x, y, z) is introduced, with the z axis being the axis of rotation. This system is fixed to the structure and spins with it.

A single time-periodic control force $P(\phi)$ is applied, as shown in Fig. 2. This concentrated force acts at a fixed node that is midway along the length of the cylinder. For future reference, the point where the load is applied is denoted Q. The force is pointing in the x direction, always remaining normal to the "surface" of the cylinder. The first four Fourier harmonics of the optimal $P(\phi)$ are sought; namely, we seek the nine constants ${}^nP$ in the finite expansion $P = \sum_{n=-4}^{4} {}^nPe^{in\phi}$ [cf. Eq. (10)].

First, we consider the case where u_x at point Q is to be minimized. Cost A is used, with no penalty imposed on the control magnitude ($r_1 = 0$). Figure 3a shows the optimal control force, and Fig. 3b shows the corresponding displacement u_x at point Q, as functions of the nondimensional time ϕ. The displacement u_x obtained with no control, i.e., as the result of the thermal loading alone, is also shown in Fig. 3b. With the optimal control, an identically zero displacement u_x at Q is achieved, as expected (see Remark 4 in Sec. II).

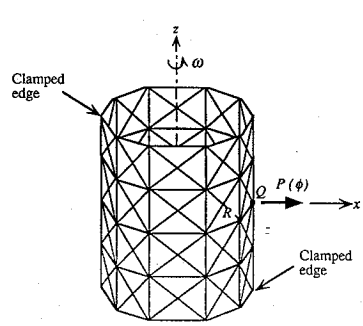

Fig. 2 Cylindrically shaped truss structure, spinning around its axis while being exposed to solar radiation. A single time-periodic force controls the thermoelastic deformation. The nodes Q and R are shown.

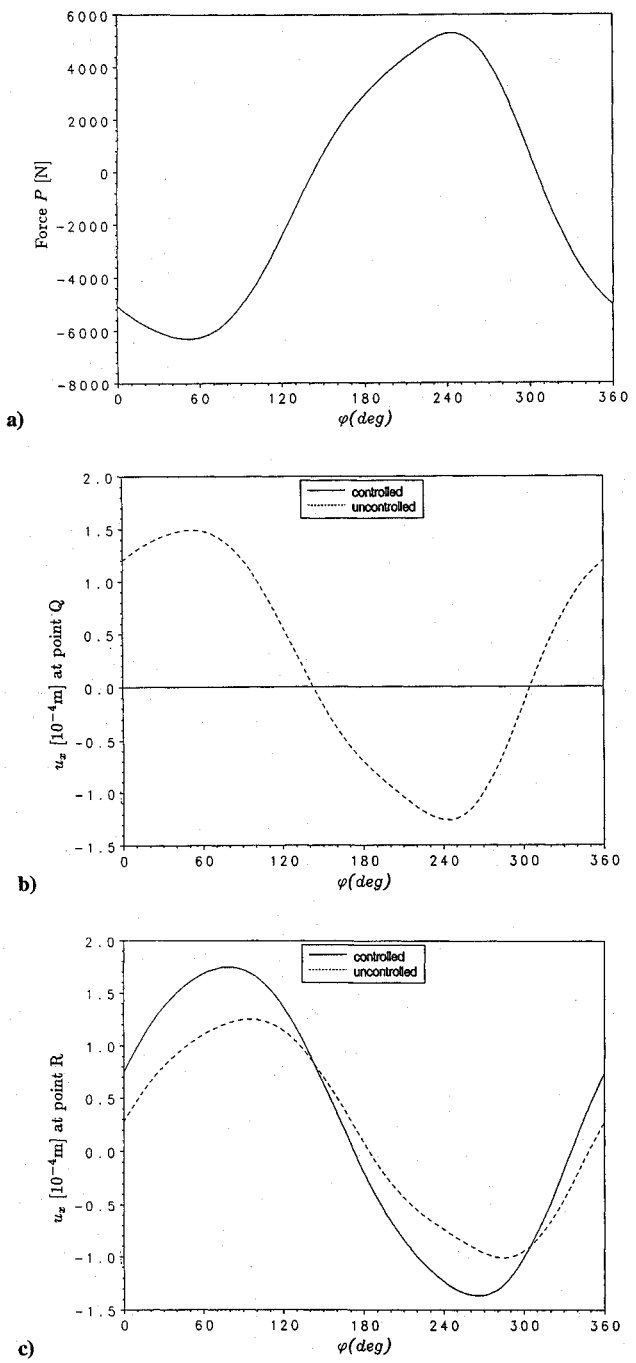

Fig. 3 Minimization of u_x at point Q (cost A, $r_1 = 0$): a) the optimal control force; b) u_x at point Q, with and without control; and c) u_x at point R, with and without control.

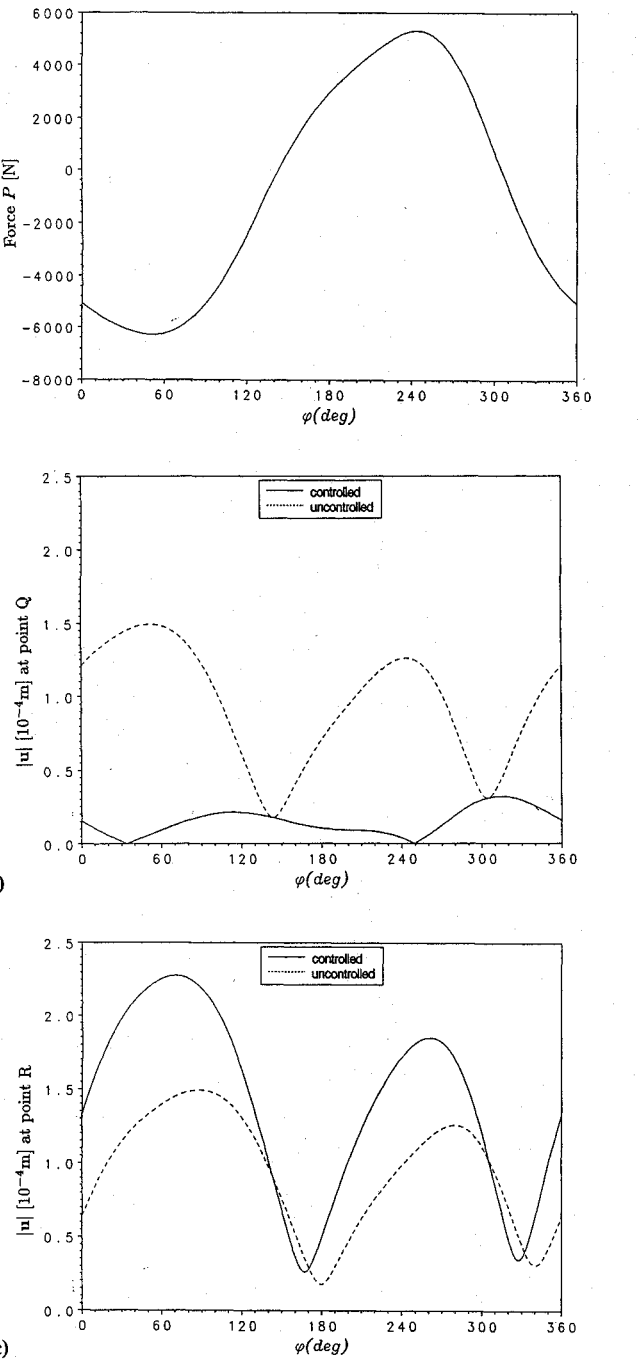

Fig. 4 Minimization of $|u|$ at point Q (cost B, $r_1 = 0$): a) the optimal control force; b) $|u|$ at point Q, with and without control; and c) $|u|$ at point R, with and without control.

However, one pays the price of larger displacements at other points. Figure 3c shows the displacement u_x, with and without control, at the node R, which is adjacent to Q on the same circumferential line (see Fig. 2). We see that the controlled displacement in larger than the uncontrolled displacement at this node during half of the period. This is an "overshoot" effect, which is particularly strong at points near the loading point Q.

Second, we try to minimize the displacement u_y at point Q. Of course, there is no sense in controlling the displacement in the y direction using a force directed orthogonally. This poor choice manifests itself in the magnitude of the optimal control load obtained; its maximum absolute value is over 5×10^9 N. Also, we get huge displacements at some other points, e.g., at R.

Next, we minimize the "total displacement" $|\boldsymbol{u}|$ at node Q. We use cost B with $r_1 = 0$. Figures 4a and 4b show the optimal control force and the displacement $|\boldsymbol{u}|$ at point Q, respectively. The optimal loads shown in Figs. 3a and 4a are almost identical; this is because the displacement component in the direction normal to the cylindrical surface (the x direction) is by far the dominant one in the thermoelastic response. Figure 4b shows that, by applying the optimal control, the maximal displacement at Q is reduced by a factor of about 5. Moreover, the figure shows that the displacement obtained with optimal control is at no point in time larger than the uncontrolled displacement. One should note that this is not guaranteed a priori since the quantity being minimized is the displacement averaged over one period of the motion [cf. Eq. (1)].

Again, there is a price to pay for reducing the displacement at point Q. Figure 4c shows the displacement $|\boldsymbol{u}|$, with and without control, at node R. The overshoot effect is prominent in this case; most of the time the controlled displacement is significantly larger than the uncontrolled displacement.

Now we use cost B again, minimizing $|\boldsymbol{u}|$ at node Q, but with a nonzero penalty on the magnitude of the control force. We assign different values to the penalty r_1 and examine the effect on

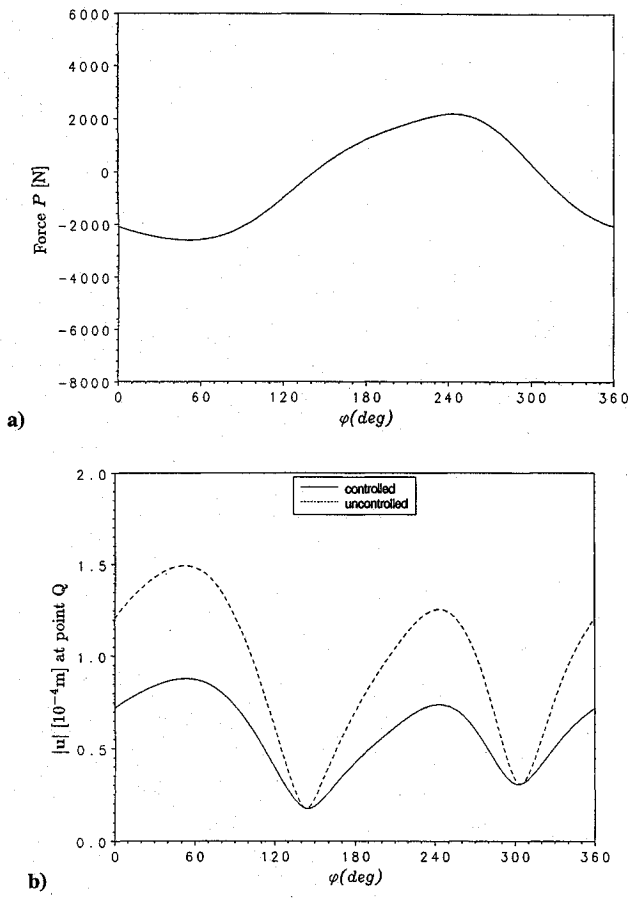

Fig. 5 Minimization of $|u|$ at point Q, with a penalty on the control magnitude [cost B, $r_1 = 0.63\,(Ep)^{-2}$]: a) the optimal control force and b) $|u|$ at point Q, with and without control.

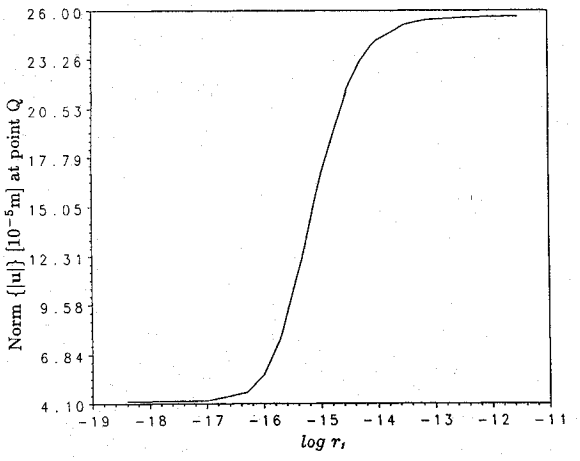

Fig. 6 Minimization of $|u|$ at point Q, with a penalty on the control magnitude (cost B, $r_1 \neq 0$): the $L_2[0, 2\pi]$ norm of $|u(\phi)|$ at point Q as a function of the penalty r_1.

the optimal load and the displacements. Figures 5a and 5b show, respectively, the optimal force and the displacement $|u|$ at point Q, with $r_1 = 0.63(E_p)^{-2}$ (m/N)^2. Because of the penalty imposed on the applied force, its magnitude is about 2.5 times smaller compared with the no-penalty case (Fig. 4a). On the other hand, the maximal displacement in Fig. 5b is about three times larger (cf. Fig. 4b) although the property that the controlled displacement is never larger than the uncontrolled displacement is maintained. It is also interesting to note that with a nonzero load penalty the displacement $|u|$ is always strictly positive, whereas Fig. 4b shows that if no load penalty is applied, then the displacement vanishes twice during the period.

Figure 6 summarizes the results obtained with various values of r_1. The $L_2[0, 2\pi]$ norm of the displacement $|u(\phi)|$ at point Q,

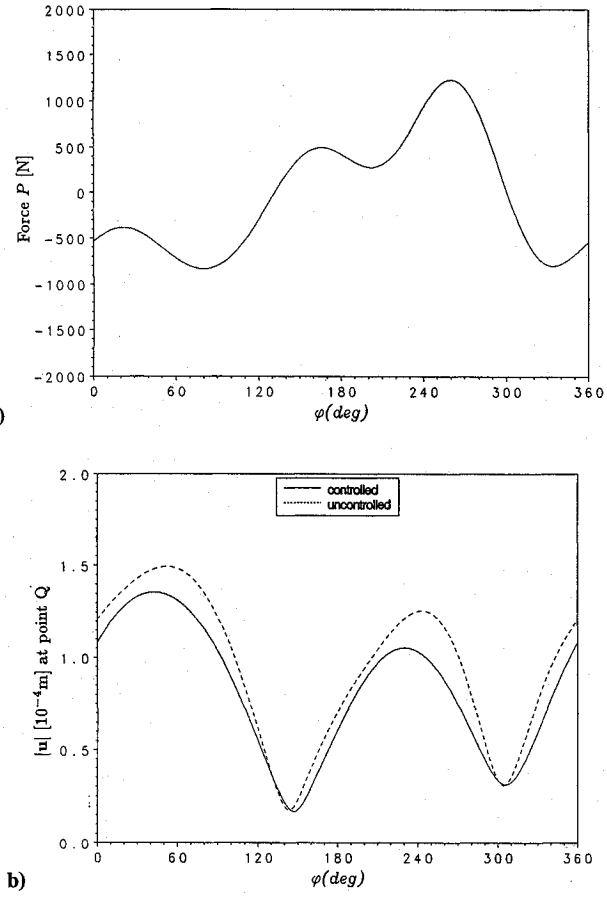

Fig. 7 Global minimization of $|u|$ (cost D, $w \equiv 1$, $r_1 = 0$): a) optimal control force and b) $|u|$ at point Q, with and without control.

defined as $(\int_0^{2\pi} |u(\phi)|^2\, d\theta)^{1/2}$, is shown as a function of the penalty r_1 in a logarithmic scale. For a very small penalty, the displacement norm approaches the value corresponding to the no-penalty case. For a very large penalty, the control loads become insignificant, and the norm approaches the value corresponding to the uncontrolled (thermally induced) displacement.

Finally we consider cost D, with $r_1 = 0$ and $w(x) \equiv 1$. This corresponds to the global minimization of the deformation throughout the structure. Figures 7a and 7b show the optimal force and the displacement $|u|$ at point Q, respectively. The loading function is much more oscillatory in this case than that obtained for the local minimization (cf. Fig. 4a), and, as expected, the reduction in the displacement at node Q is much less dramatic (cf. Fig. 4b).

V. Concluding Remarks

We have devised an effective numerical scheme for the open-loop optimal control of the thermoelastic deformation of space structures undergoing periodic motion. The scheme has been applied to a simple truss-type structure. The optimization scheme is highly compatible with the numerical method of analysis in which finite element discretization in space and discrete Fourier decomposition in time are combined.

Extensions of the scheme are appropriate in two different directions, namely, in the control-related context and in the thermostructural model. As far as the former is concerned, more elaborated case studies are needed, including the use of several actuators operating simultaneously. The design of a corresponding closed-loop control may be considered. In addition, one may attempt to find the optimal choice for the location and orientation of the controls, under given constraints. Both of these would require a much heavier use of the classical tools of control theory. Also, the possibility of reducing the thermoelastic deformations through thermal control rather than mechanical control is to be investigated.

The second type of extension concerns the structural model under consideration. More complicated thermoelastic models serving

as the basis for the load optimization may be considered. These may include, for example, dynamic thermoelastic coupling effects, temperature-dependent material properties, radiation exchange among different parts of the structure, and more complicated types of structures such as shells.

Acknowledgments

This work was supported in part by the Adler Fund for Space Research managed by the Israel Academy of Sciences. We are also grateful to Y. Oshman for his helpful remarks and to A. Andel for his assistance in programming.

References

[1]Clark, S. C., and Allen, G. E., "Thermo-Mechanical Design and Analysis System for the Hughes 76-In. Parabolic Antenna Reflector," *Spacecraft Thermal Control, Design and Operation*, edited by H. E. Collicott and P. E. Bauer, AIAA, New York, 1983, pp. 109–129.

[2]Nour-Omid, S., Nour-Omid, B., and Rankin, C. C., "Large Rotation Transient Analysis of Flexible Space Structures," *Proceedings of the Second World Congress on Computational Mechanics* (Stuttgart, Germany), 1990, pp. 67–70.

[3]Thornton, E. A., Dechaumphai, P., and Wieting, A. R., "Integrated Finite Element Thermal-Structural Analysis with Radiation Heat Transfer," *Proceedings of the 23rd Structures, Structural Dynamics and Materials Conference*, Pt. 1, AIAA, New York, 1982, pp. 188–196.

[4]Thornton, E. A., and Paul, D. B., "Thermal-Structural Analysis of Large Space Structures: An Assessment of Recent Advances," *Journal of Spacecraft and Rockets*, Vol. 22, No. 4, 1985, pp. 385–393.

[5]Nash, W. A., and Lardner, T. J., "Parametric Investigation of Factors Influencing the Mechanical Behavior of Large Space Structures," Air Force Office of Scientific Research, Rept. TR-86-0858, 1985.

[6]Hedgepeth, J. M., and Miller, R. K., "Structural Concepts for Large Solar Concentrators," *Acta Astronautica*, Vol. 17, Jan. 1988, pp. 79–89.

[7]Peskett, S. C., and Gethin, D. T., "Thermal Analysis of Spacecraft," *Numerical Methods in Thermal Problems*, edited by R. W. Lewis and K. Morgan, Vol. VI, Pt. 1, Pineridge Press, 1989, pp. 713–729.

[8]Mahaney, J., and Thornton, E. A., "Self-Shadowing Effects on the Thermal-Structural Response of Orbiting Trusses," *Journal of Spacecraft and Rockets*, Vol. 24, No. 4, 1987, pp. 342–448.

[9]Ko, W. L., "Solution Accuracies of Finite Element Reentry Heat Transfer and Thermal Stress Analyses of Space Shuttle Orbiter," *International Journal for Numerical Methods in Engineering*, Vol. 25, No. 2, 1988, pp. 517–543.

[10]Mahaney, J., Thornton, E. A., and Dechaumphai, P., "Integrated Thermal-Structural Analysis of Large Space Structures," *Computational Aspects of Heat Transfer in Structures Symposium*, NASA Langley Research Center, NASA CP-2216, Hampton, VA, 1981, pp. 179–198.

[11]Lutz, J. D., Allen, D. H., and Haisler, W. E., "Finite-Element Model for the Thermoelastic Analysis of Large Composite Space Structures," *Journal of Spacecraft and Rockets*, Vol. 24, No. 5, 1987, pp. 430–436.

[12]Rand, O., and Givoli, D., "Thermal Analysis of Space Trusses Including Three-Dimensional Effects," *International Journal for Numerical Methods in Heat and Fluid Flow*, Vol. 2, No. 2, 1992, pp. 115–125.

[13]Givoli, D., and Rand, O., "Harmonic Finite-Element Thermoelastic Analysis of Space Frames and Trusses," *Journal of Thermal Stresses* (to be published).

[14]Rand, O., and Givoli, D., "A Finite Element Spectral Method with Application to the Thermoelastic Analysis of Space Structures," *International Journal of Numerical Methods in Engineering*, Vol. 30, No. 2, 1990, pp. 291–306.

[15]Givoli, D., and Rand, O., "Thermoelastic Analysis of Space Structures in Periodic Motion," *Journal of Spacecraft and Rockets*, Vol. 28, No. 4, 1991, pp. 457–464.

[16]Joshi, S. M., *Control of Large Flexible Space Structures*, Springer–Verlag, Berlin, 1989.

[17]Chatterjee, A. K., "Optimal Orbit Transfer Suitable for Large Flexible Structures," *Journal of the Astronautical Sciences*, Vol. 37, No. 3, 1989, pp. 261–280.

[18]Young, K. D., "Distributed Finite-Element Modeling and Control Approach for Large Flexible Structures," *Journal of Guidance, Control, and Dynamics*, Vol. 13, No. 4, 1990, pp. 703–713.

[19]Kamat, M. P. (ed.), *Optimization Issues in the Design and Control of Large Space Structures*, American Society of Civil Engineers, New York, 1985.

[20]Atluri, S. N., and Amos, A. K. (eds.), *Large Space Structures: Dynamics and Control*, Springer–Verlag, Berlin, 1988.

[21]Speyer, J. L., "On the Fuel Optimality of Cruise," *Journal of Aircraft*, Vol. 10, No. 12, 1973, pp. 763–765.

[22]Speyer, J. L., and Evans, R. T., "A Second Variational Theory for Optimal Periodic Processes," *IEEE Transactions on Automatic Control*, Vol. AC-29, No. 2, 1984, pp. 138–147.

[23]Wang, Q., and Speyer, J. L., "Necessary and Sufficient Conditions for Local Optimality of a Periodic Process," *SIAM Journal of Control and Optimization*, Vol. 28, No. 2, 1990, pp. 482–497.

[24]Gilbert, E. G., "Optimal Periodic Control: A General Theory of Necessary Conditions," *SIAM Journal of Control and Optimization*, Vol. 15, No. 5, 1977, pp. 1–28.

[25]Hughes, T. J. R., *The Finite Element Method*, Prentice–Hall, Englewood Cliffs, NJ, 1987.

E. A. Thornton
Associate Editor